

AD-A241 918



✓ m (2)

NAVAL POSTGRADUATE SCHOOL Monterey, California

DTIC
1000000



THESIS

WATER VAPOR INFLUENCE ON
SATELLITE-MEASURED AEROSOL
CHARACTERISTICS

by

Timothy P. Mahony

March 1991

Thesis Advisor:

P. A. Durkee

Approved for public release; distribution is unlimited.

91 10 22 085

91-14275



REPORT DOCUMENTATION PAGE

1a. REPORT SECURITY CLASSIFICATION UNCLASSIFIED		1b. RESTRICTIVE MARKINGS	
2a. SECURITY CLASSIFICATION AUTHORITY		3. DISTRIBUTION/AVAILABILITY OF REPORT Approved for public release; distribution is unlimited.	
2b. DECLASSIFICATION/DOWNGRADING SCHEDULE			
4. PERFORMING ORGANIZATION REPORT NUMBER(S)		5. MONITORING ORGANIZATION REPORT NUMBER(S)	
6a. NAME OF PERFORMING ORGANIZATION Naval Postgraduate School	6b. OFFICE SYMBOL (If Applicable) 63	7a. NAME OF MONITORING ORGANIZATION Naval Postgraduate School	
6c. ADDRESS (city, state, and ZIP code) Monterey, CA 93943-5000		7b. ADDRESS (city, state, and ZIP code) Monterey, CA 93943-5000	
8a. NAME OF FUNDING/SPONSORING ORGANIZATION	6b. OFFICE SYMBOL (If Applicable)	9. PROCUREMENT INSTRUMENT IDENTIFICATION NUMBER	
8c. ADDRESS (city, state, and ZIP code)		10. SOURCE OF FUNDING NUMBERS	
		PROGRAM ELEMENT NO.	PROJECT NO.
		TASK NO.	WORK UNIT ACCESSION NO.
11. TITLE (Include Security Classification) WATER VAPOR INFLUENCE ON SATELLITE-MEASURED AEROSOL CHARACTERISTICS			
12. PERSONAL AUTHOR(S) Mahony, Timothy Patrick			
13a. TYPE OF REPORT Master's Thesis	13b. TIME COVERED FROM TO	14. DATE OF REPORT (year, month, day) 1991 March	15. PAGE COUNT 52
16. SUPPLEMENTARY NOTATION The views expressed in this thesis are those of the author and do not reflect the official policy or position of the Department of Defense or the U.S. Government.			
17. COSATI CODES		18. SUBJECT TERMS (continue on reverse if necessary and identify by block number)	
FIELD	GROUP	SUBGROUP	
		Satellite, Aerosol, Radiative Processes, Remote Sensing	
19. ABSTRACT (Continue on reverse if necessary and identify by block number) This study demonstrates the significance of water vapor's influence on satellite-retrieved aerosol characteristics using NOAA's AVHRR. An improvement to optical depth and Aerosol Particle Size Index (S ₁₂) estimations derived from channels 1 (0.63μm) and 2 (0.86μm), is made through knowledge of column water vapor derived from channels 4 (10.8μm) and 5 (12.0μm). A 2.0 gm cm ⁻² column water vapor produces a 5% increase in S ₁₂ . This results in a 15% error in the variable scattering phase function P(Θ) and retrieved aerosol optical depth (δa). The error introduced by water vapor is quantified through use of the LOWTRAN7 atmospheric propagation model to be applied as a reformulated parameterization of (P(Θ)).			
20. DISTRIBUTION/AVAILABILITY OF ABSTRACT <input checked="" type="checkbox"/> UNCLASSIFIED/UNLIMITED <input type="checkbox"/> SAME AS RPT. <input type="checkbox"/> DTIC USERS		21. ABSTRACT SECURITY CLASSIFICATION Unclassified	
22a. NAME OF RESPONSIBLE INDIVIDUAL P. A. Durkee		22b. TELEPHONE (Include Area Code) (408) 646-3465	22c. OFFICE SYMBOL 63De

Approved for public release; distribution is unlimited.

Water Vapor Influence On Satellite-Measured Aerosol Characteristics

by

Timothy Patrick Mahony
Lieutenant, United States Navy
B.S., United States Naval Academy, 1983

Submitted in partial fulfillment of the requirements
for the degree of

**MASTER OF SCIENCE IN METEOROLOGY AND
PHYSICAL OCEANOGRAPHY**

from the

NAVAL POSTGRADUATE SCHOOL
March 1991

Author:



Timothy Patrick Mahony

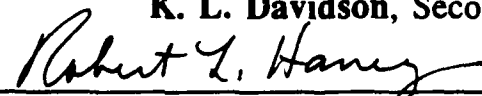
Approved by:



P. A. Durkee, Thesis Advisor



K. L. Davidson, Second Reader



Robert L. Haney, Chairman, Department of Meteorology

ABSTRACT

This study demonstrates the significance of water vapor's influence on satellite-retrieved aerosol characteristics using NOAA's AVHRR. An improvement to optical depth and Aerosol Particle Size Index (S_{12}) estimations derived from channels 1 ($0.63\mu\text{m}$) and 2 ($0.86\mu\text{m}$), is made through knowledge of column water vapor derived from channels 4 ($10.8\mu\text{m}$) and 5 ($12.0\mu\text{m}$). A 2.0 gm cm^{-2} column water vapor produces a 5% increase in S_{12} . This results in a 15% error in the variable scattering phase function $P(\Theta)$ and retrieved aerosol optical depth (δ_a). The error introduced by water vapor is quantified through use of the LOWTRAN7 atmospheric propagation model to be applied as a reformulated parameterization of $P(\Theta)$.



SEARCHED
SERIALIZED
INDEXED
FILED
APR 1984
FBI - MEMPHIS
A-1

TABLE OF CONTENTS

I. INTRODUCTION.....	1
A. PURPOSE.....	1
B. MOTIVATION.....	2
C. THE MODEL.....	3
II. THEORY.....	5
A. PARTICLE SIZE INDEX (S_{12}).....	5
B. WATER VAPOR ABSORPTION IN THE VISIBLE / NEAR INFRA-RED.....	10
C. BRIGHTNESS TEMPERATURE DIFFERENCE (T_4-T_5).....	14
III. PROCEDURE.....	20
A. INTRODUCTION.....	20
B. OVERVIEW.....	20
C. INPUT CHARACTERISTICS.....	24
1. Optical Depth Profiles.....	25
2. Water Vapor.....	26
3. Surface Temperature.....	28
D. PROCEDURAL SUMMARY.....	28
IV. RESULTS.....	30
A. THE EFFECT OF AEROSOL OPTICAL DEPTH VARIATIONS ON S_{12}	30
1. Multiple $\delta_a(\lambda)$ Scheme.....	30
2. Parallel $\delta_a(\lambda)$ Scheme.....	30
B. THE EFFECT OF SURFACE TEMPERATURE VARIATIONS ON THE T_4-T_5 REPRESENTATION OF W.....	30
C. THE W CORRECTION TO S_{12}	34
1. Graphical Application.....	34
2. The Reformulated Parameterization.....	36

D. SINGLE VERSUS MULTIPLE SCATTERING	36
V. CONCLUSIONS.....	38
LIST OF REFERENCES.....	40
INITIAL DISTRIBUTION LIST.....	42

LIST OF TABLES

Table 1 NOAA-7 AVHRR Channel Bandwidths.....	5
Table 2 Model Output Coefficients Applied To Dalu's Theory ($w = A(T_4 - T_5)$).....	34

LIST OF FIGURES

Fig. 1 Extinction formulation as a function of particle radius for channels 1 (solid) and 2 (dash). Modified from Durkee (1984).....	9
Fig. 2 NOAA-7 AVHRR channel 1 and 2 response functions and total atmospheric radiance.....	11
Fig. 3 NOAA-7 AVHRR channel 1 and 2 response functions and atmospheric transmittance due to water vapor.....	12
Fig. 4 NOAA-7 AVHRR channel 1 and 2 response functions and the influence of water vapor on atmospheric radiance.....	13
Fig. 5 NOAA-7 AVHRR channel 4 and 5 response functions and atmospheric transmittance due to water vapor.....	16
Fig. 6 Total water vapor content (kg/m ²) as a function of brightness temperature difference from Dalu (1986).....	18
Fig. 7 Comparison of water vapor content from ships with radiative transfer model runs using ship radiosonde data. From Dalu (1986).....	19
Fig. 8 Flow chart of model run.....	21
Fig. 9 NOAA-7 AVHRR filter function response curves.....	23
Fig. 10 Multiple optical depth profiles (M).....	26
Fig. 11 Parallel optical depth profiles (P).....	27
Fig. 12 S ₁₂ versus column water vapor (w) for the multiple optical depth scheme (M).....	31
Fig. 13 S ₁₂ versus column water vapor (w) for the parallel optical depth scheme (P).....	32
Fig. 14 T ₄ -T ₅ versus column water vapor (w) for a variety of surface temperatures.....	33
Fig. 15 S ₁₂ correction for column water vapor.....	35
Fig. 16 S ₁₂ normalized by S ₁₂ (dry).....	37

ACKNOWLEDGMENTS

The author wishes to recognize the key players, without whom, this endeavor might have become a struggle. The top of this list has to be my wife, Mary, who has dealt with many of the worlds problems, so that I didn't have to. I am grateful to: Professor Philip A. Durkee, for his consistent demeanor and patience despite my continual knocking at his door; Professor Kenneth L. Davidson, for particularly quick turnarounds as a reader; and Professor Curtis A. Collins of the Oceanography Department, for allowing me to use his computer. I want to be sure to thank Mr. Craig Motell, for always being available for programming support.

I. INTRODUCTION

A. PURPOSE

Direct measurements of aerosol characteristics can be provided by ship or aircraft. Although they provide valuable information, they are very expensive, require detailed coordination, and only small sections of the world's oceans can be monitored at any time. Satellites can provide near continuous spatial and temporal data desirable for evaluating large scale global effects as well as timely local measurements suitable for military applications. Meteorological satellites, however, have been designed to measure cloud albedos while much lower radiances are associated with aerosol optical depth variations (Durkee 1984). Therefore, careful processing of satellite data is necessary to determine aerosol characteristics.

Frost (1988) has developed an algorithm to derive aerosol particle characteristics from the Advanced Very High Resolution Radiometer (AVHRR) on the NOAA polar orbiting satellites. By taking advantage of the varying sensitivities of aerosol scattering in two spectral windows, a multi-channel comparison provides information about the aerosol particle size distribution. By applying this information to a variable scattering phase function, improved estimations of optical depth are possible.

This study will provide an improvement to Frost's technique. Frost requires analyzed pixels to be free of clouds. However, these clear pixels still contain varying amounts of water vapor. Frost assumes that varying amounts of water vapor do not appreciably effect retrieved radiances. This study will use the U. S.

Air Force's **LOWTRAN7** atmospheric propagation model to demonstrate the degree that water vapor influences present aerosol estimations.

This thesis will:

1. Show the effect of varying water vapor amounts on satellite-retrieved aerosol characteristics, specifically the particle size index parameter or **S₁₂** as defined by Frost (1988).
2. Provide a parameterization of **S₁₂** corrected for column water vapor (**w**), using a multichannel analysis of **AVHRR** data.

B. MOTIVATION

Radiation in the atmosphere is attenuated by many processes. It is absorbed and scattered by molecules, aerosols, and meteorological features such as clouds, fog, and precipitation. Some of these influences may be of short duration and of local scale such as a cumulus cloud passing overhead and casting a shadow. Others, such as stratospheric dust particles are semipermanent and of global proportions.

Aerosols are solid or liquid particles dispersed in the atmosphere. Dust, smoke, and even fog or rain are examples of aerosols. Aerosol particles are present in the atmosphere in various forms and concentrations. In this thesis, the change in particle size due to coalescence of water vapor will not be considered.

With the ever increasing use of electro-optical devices, military applications benefit significantly from improved aerosol measurements. The optimum waveband for a laser is from 0.4 to 1.0 μm . This waveband avoids ozone absorption at shorter wavelengths, as well as the water vapor absorption that dominates longer wavelengths (Bloembergen, et al 1987). This waveband, however, is significantly influenced by aerosol scattering.

Another important hypothesis that demonstrates the need for better aerosol estimations and modeling on a much larger scale is that of Charlson, et al. (1987). Charlson proposes that the major source of cloud condensation nuclei (CCN) over remote unpolluted oceans appears to be aqueous dimethylsulphide gas (DMS) produced by phytoplankton as a waste product. DMS is emitted through the sea surface through a chain of complex biological and chemical processes where it is oxidized in the atmosphere to form sulfate aerosol particles which act as CCN. Increased phytoplankton populations and the resulting increase in aerosol particles effectively cool the atmosphere by increasing backscatter to space. A 30% increase in aerosols over the ocean surfaces worldwide can conservatively decrease the average global temperature by 1.3 K (Charlson 1987).

For many applications, aerosols result in noise interfering with measurements of other processes. These applications benefit from improved aerosol estimations that eliminate aerosol contamination of the data.

C. THE MODEL

LOWTRAN7 (Low Resolution Transmittance) is a model that calculates atmospheric transmittance, scattering and absorption. It incorporates separate molecular profiles for all major as well as 13 minor and trace gases, all as a function of altitude (0 to 100km). Representative atmospheric aerosol, cloud, and rain models are provided with the ability to replace any or all values with theoretical or measured data at the discretion of the user. The model also provides six reference atmospheres with options to redefine or retain profiles.

LOWTRAN7 is a band model. Average transmittance is calculated over 20 cm^{-1} bands. The band parameters have been determined semi-empirically

determined semi-empirically through the averaging of line parameters. In principle, the line by line method is available, but the calculations are too elaborate and time consuming for most users. Some accuracy is gained by a line method, but it is not significant enough to warrant the loss of efficiency. Individual lines within a band may vary significantly, yet it is fair to characterize the effective band parameters through the averaging of line parameters so long as a specific line result is not desired.

For use in multiwavelength applications (ie. satellites) the appropriate spectral response functions for the sensor can be applied to the output data through **LOWFIL7** (**LOWTRAN7**'s filter program). The data set derived through the running of the main program is filtered through the sensor's response function and produces a normalized radiance estimate of the sensor measurement.

II. THEORY

A. PARTICLE SIZE INDEX (S_{12})

The Advanced Very High Resolution Radiometer (AVHRR) has been a part of all the NOAA polar orbiting satellites. It has five channels:

TABLE 1
NOAA-7 AVHRR CHANNEL BANDWIDTHS

<u>Channel #</u>	<u>Bandwidth (μm)</u>
1	0.58 - 0.68
2	0.725 - 1.10
3	3.55 - 3.93
4	10.30 - 11.30
5	11.50 - 12.50

AVHRR satellite detected radiances in the red-visible (chan. 1) and the near infra-red (chan. 2) wavelength ranges have been found to be positively correlated with aerosol optical depth (δ) (Durkee 1984; Griggs 1979).

Using a single scattering approximation and knowing that optical depths over the ocean are small (Pfeil 1986), Frost (1988) used a simplified form of the Radiative Transfer Equation (RTE):

$$L(\delta, \mu, \phi) \sim \frac{\omega_0 \cdot F_0}{4\mu} \cdot p(\Theta) \cdot \delta \quad (2.1)$$

where, L = diffuse radiance,
 ω_0 = single scatter albedo,

F_0 = solar radiative flux,
 $\mu = \cos\theta$ (θ = satellite zenith angle),
 p = scattering phase function,
 Θ = single scattering angle,
 δ = optical depth.

In an optically thin (small δ) atmosphere, multiple scattering effects are very small, making single scattering a reasonable assumption (Frost 1988).

There are three primary sources of upwelled radiance (L) that contribute to satellite detected radiance in the red-visible and near-infrared wavelengths. The contributions can be expressed as:

$$L = L_a + L_r + L_s \quad (2.2)$$

where L_a is aerosol scatter, L_r is molecular or Rayleigh scatter, the wavelength of radiation is much greater than the size of the scattering material, and L_s is sea surface reflectance. Except for sunglint, L_s is very small for red wavelengths (albedo = 0.5%) and zero for wavelengths greater than $0.7\mu\text{m}$ (Ramsey 1968). Therefore, as long as sunglint geometry is avoided, total radiance is due to the sum of aerosol and molecular scattering effects ($L \approx L_a + L_r$).

L_r is strongly wavelength (λ) dependant, but does not vary spatially. Therefore L_r forms a baseline $L(\lambda)$ and aerosol particles are the dominant source of upwelled radiance variations ($\Delta L \sim \Delta L_a$). From Eqn. 2.1, changes in satellite measured radiance are directly determined from changes in aerosol characteristics like ω_0 , $p(\Theta)$, and aerosol optical depth (δ_a). Therefore, to retrieve a more accurate δ from L_a measurements, knowledge of $p(\Theta)$ variations is required.

Durkee (1984) showed that retrieved radiances at red wavelengths (chan. 1) are more sensitive to varying densities of small aerosol particles than that of near-infrared (nir) wavelengths (chan. 2). The most significant parameter contributing to retrieved radiances at AVHRR channel 1 and 2 wavelengths is the extinction coefficient (σ_{ext}) and specifically the vertical integral of σ_{ext} or the optical depth (δ).

$$\delta = \int_0^H \sigma_{\text{ext}} dz \quad (2.3)$$

σ_{ext} is the sum of extinction due to absorption (σ_{abs}) and due to scattering (σ_{scat}). For marine aerosols, absorption is negligible, therefore $\sigma_{\text{ext}} = \sigma_{\text{scat}}$ and

$$\delta = \int_0^H \sigma_{\text{scat}} dz. \quad (2.4)$$

Three terms contribute to σ_{scat} :

$$\sigma_{\text{scat}} = \int_0^{\infty} \pi r^2 \cdot Q_{\text{scat}}(m, \lambda, r) \cdot n(r) dr \quad (2.5)$$

where, πr^2 = particle cross sectional area,

$Q_{\text{scat}}(m, \lambda, r)$ = scattering efficiency,

m = complex index of refraction,

λ = wavelength,

r = particle radius,

$n(r)$ = number distribution of particles.

Figure 1 shows the influence of the terms of Eqn. 2.5 as a function of r and the resulting number-weighted extinction ($\pi r^2 \cdot Q_{\text{scat}} \cdot n(r)$) for channel 1 and channel 2. Scattering cross section ($\pi r^2 \cdot Q_{\text{scat}}$) and the particle size distribution ($n(r)$) for a modeled distribution of marine particles at 80% RH are plotted. As wavelength increases, so does the r of most efficient scattering (Q_{scat}). The result is a shift in the scattering cross section and a similar shift in the r that most significantly contributes to σ_{scat} , and therefore L at a given λ . Therefore, the slope of $L(\lambda)$ closely resembles the slope of $\delta(\lambda)$, and is similar to the slope of the aerosol particle size distribution ($n(r)$). Since aerosol particles most effectively scatter radiation at a wavelength similar to the radius of the particle, an increase in the number of small aerosol particles will increase the ratio of L_{ch1} to L_{ch2} , and the spectral variation can be quantified:

$$\frac{L_{\text{(red)}}}{L_{\text{(nir)}}} \approx \frac{L_{\text{(ch1)}}}{L_{\text{(ch2)}}} \approx \frac{\frac{\omega_0 \cdot F_0}{4\mu} \cdot p(\Theta) \cdot \delta_{\text{(ch1)}}}{\frac{\omega_0 \cdot F_0}{4\mu} \cdot p(\Theta) \cdot \delta_{\text{(ch2)}}} = \frac{\delta_{\text{(red)}}}{\delta_{\text{(nir)}}} \quad (2.6)$$

This ratio is called the Particle Size Index (S_{12}) (Frost 1988):¹

$$S_{12} = \frac{(L)_{\text{red}}}{(L)_{\text{nir}}} = \frac{(\delta)_{\text{red}}}{(\delta)_{\text{nir}}} \quad (2.7)$$

¹While Frost removed L_r prior to taking the ratio, it will not be removed in this study. It shall be accounted for in the parameterization of $p(\Theta)$.

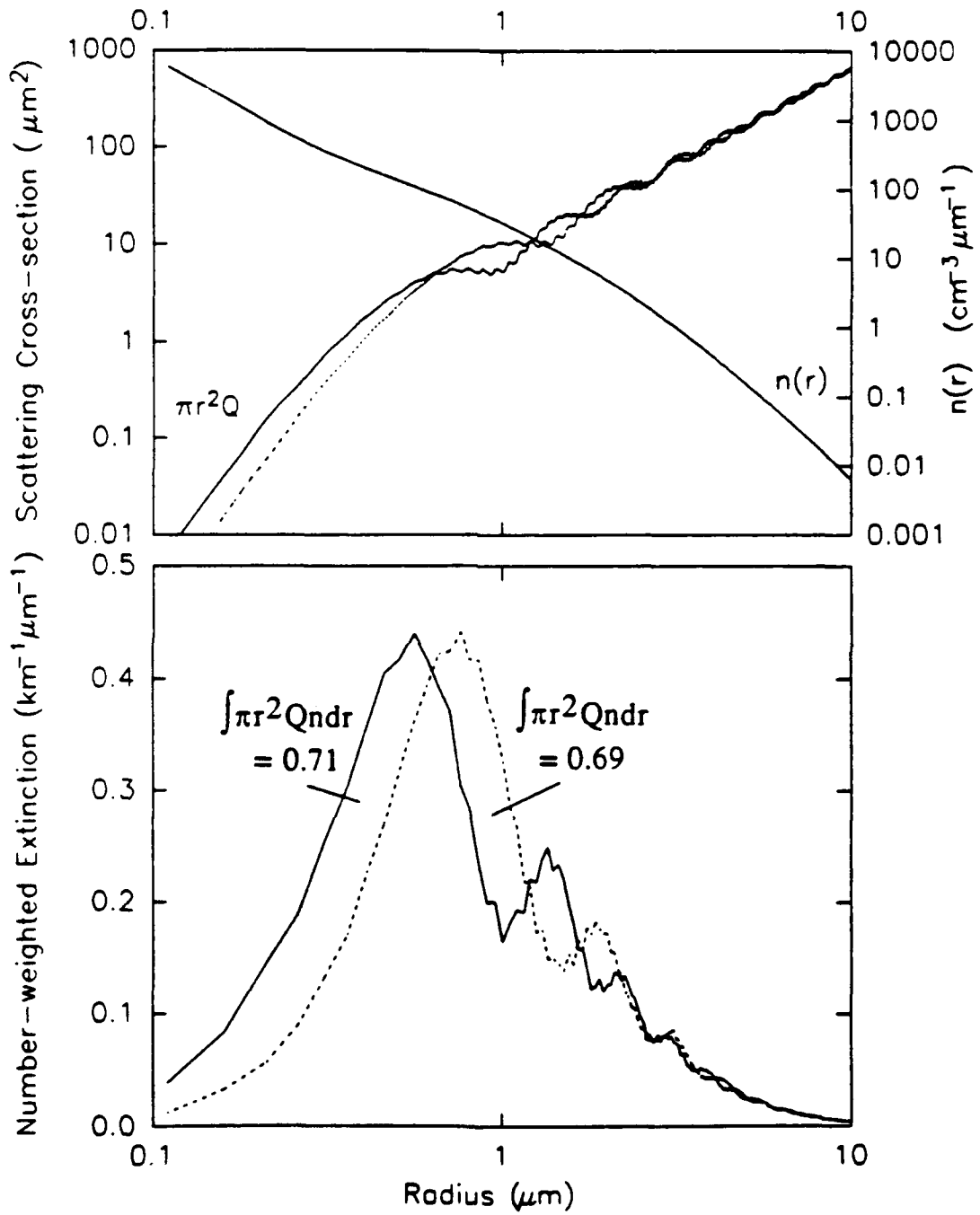


Fig. 1 Extinction formulation as a function of particle radius for channels 1 (solid) and 2 (dash). Modified from Durkee (1984).

Satellite measured radiances therefore cannot provide the actual particle size distribution, but the S_{12} gives the slope of the size distribution curve. In general, the greater the contribution of smaller particles, the larger the ratio.

Figure 2 shows a plot of NOAA-7 AVHRR channel 1 and channel 2 response function curves superimposed on LOWTRAN7's Tropical model atmosphere output radiances ($L(\lambda)$). Although as this paper will show, water vapor absorption does effect S_{12} , the dominant variable influencing $L(\lambda)$ in these wavelength bands is aerosol scattering. For the red and near-infrared region of the spectrum, variances in $L(\lambda)$ are proportional to changes in $\delta_a(\lambda)$ and therefore aerosol scattering. Note that $L(\lambda)$ in the channel 1 window (short wavelengths, small particle scattering) is greater than that of channel 2. This is primarily due to the slope of $L_r(\lambda)$ and leads to an S_{12} ratio that is generally greater than 1.

B. WATER VAPOR ABSORPTION IN THE VISIBLE / NEAR INFRA-RED

Although aerosol scattering is the dominant influence on satellite retrieved radiances at visible and near-infrared wavelengths, the role of atmospheric water vapor is not insignificant. The magnitudes of the overall L in these wavelengths are not appreciably effected, but often the goal of using satellites to estimate aerosol particle characteristics is to look for variations, which are an order of magnitude smaller than the total L .

In order to observe sometimes subtle, yet often significant trends such as global climate variations, an improvement in the accuracy of aerosol estimations is necessary.

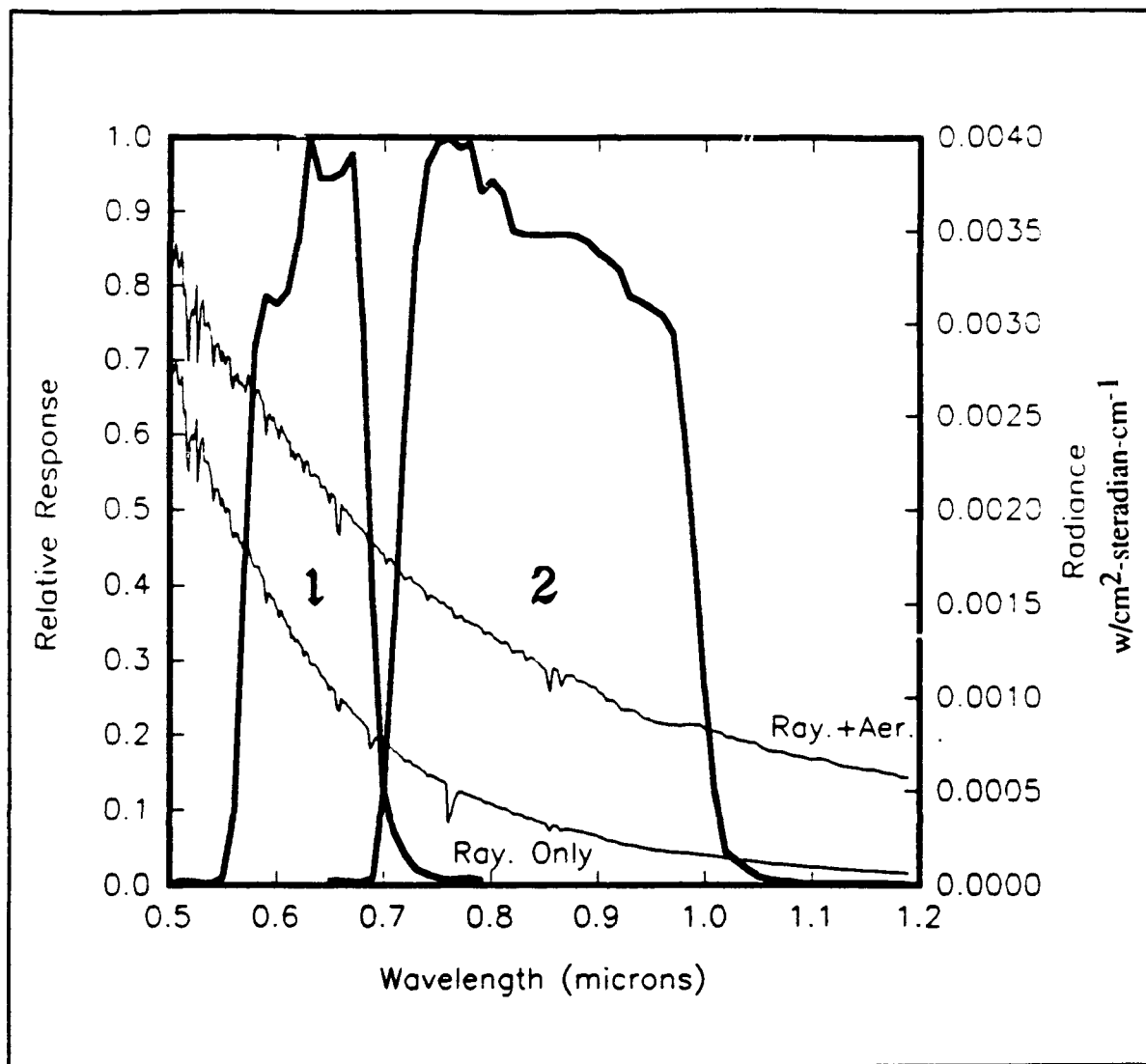


Fig. 2 NOAA-7 AVHRR channel 1 and 2 response functions and total atmospheric radiance.

Figure 3 shows the effect of water vapor alone on τ for AVHRR channels 1 and 2. Notice that for channel 1, τ is greater than channel 2, meaning that less absorption is taking place. This would tend to decrease L_2 more than L_1 and thus lead to an over-estimate of the S_{12} . Therefore a change in water vapor in a region may be misconstrued as a change in aerosol characteristics or disguise a

significant change. This implies that we might expect to see a minimum $S_{12}(w)$ at $w = \text{zero}$, and an increase in $S_{12}(w)$ with w .

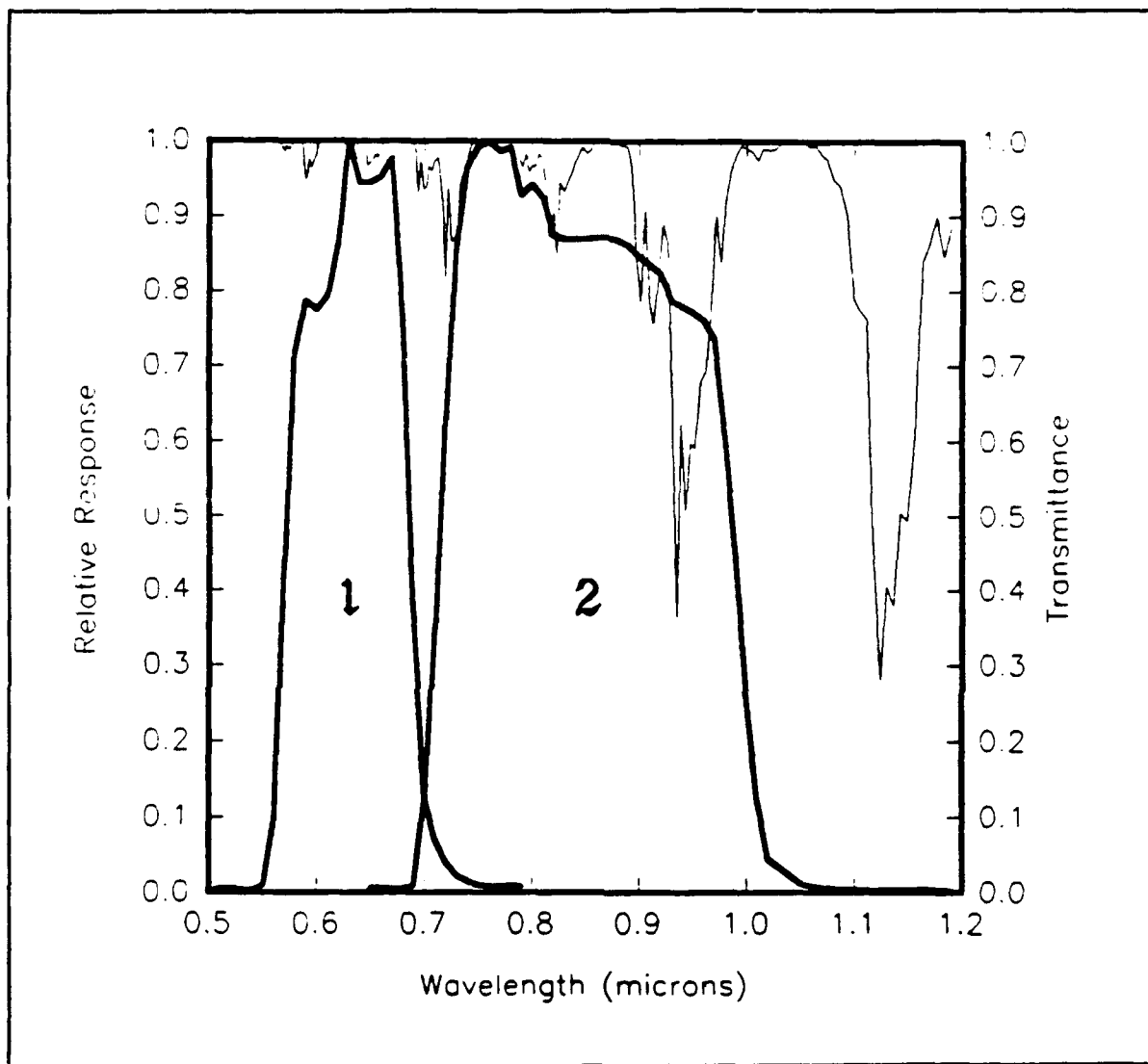


Fig. 3 NOAA-7 AVHRR channel 1 and 2 response functions and atmospheric transmittance due to water vapor.

In Figure 4, the influence of water vapor is again demonstrated when water vapor is added to LOWTRAN7's Tropical atmosphere model. Notice that while radiances decrease in both channel wavebands, channel 2 is more significantly effected. This again will cause S_{12} to increase with w even though

L_1 and L_2 decrease. There does appear to be some increase in L below $0.6 \mu\text{m}$. This is most likely due to an effective shift in particle size due to coalescence of water vapor. This study intends to look at the influence of water vapor alone on retrieved radiances, and aerosol growth will be inhibited.

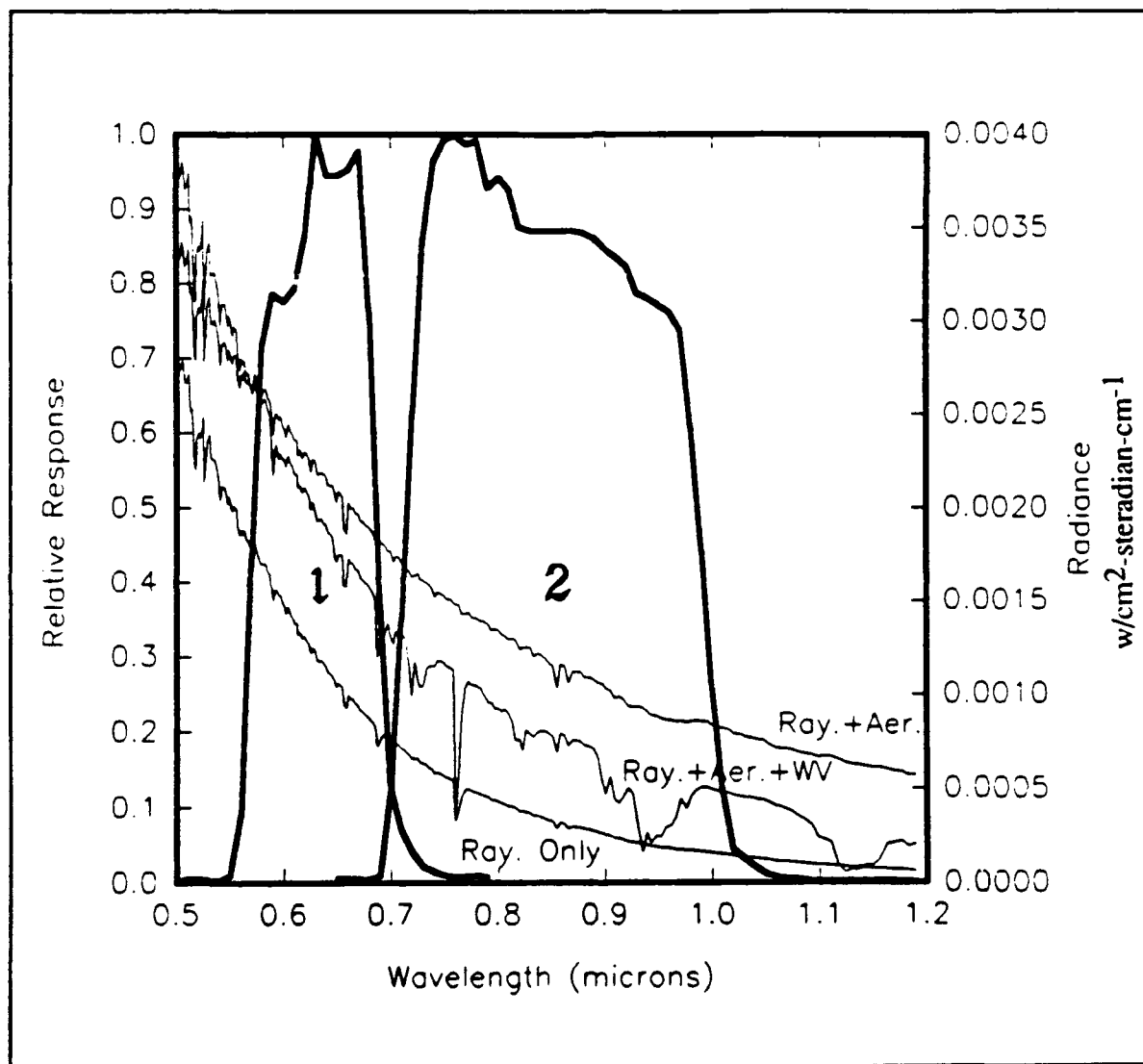


Fig. 4 NOAA-7 AVHRR channel 1 and 2 response functions and the influence of water vapor on atmospheric radiance.

C. BRIGHTNESS TEMPERATURE DIFFERENCE (T₄-T₅)

In order to take advantage of the water vapor parameterization of the scattering phase function proposed in this study, some method of measuring the water vapor present would be required.

A significant benefit of using the AVHRR is that while channels 1 and 2 provide information on optical depth variations, channels 4 and 5 in the 10 to 13 μm window region have demonstrated usefulness in atmospheric water vapor retrieval.

Unlike the aerosol backscattering of channels 1 and 2, the brightness temperature is the result of single direction radiation transfer, from the sea surface to the sensor. Therefore, τ is directly proportional to retrieved T , with absorption reducing the radiance reaching the sensor.

From Dalu, et al. (1981):

$$T_s = T_\alpha + g(w)(T_\alpha - T_\beta) \quad (2.8)$$

T_s = Sea Surface Temperature (SST)

T_α = Brightness Temp. of most transparent channel

T_β = Brightness Temp. of second channel

$g(w)$ = function of water vapor content

$$= \left[\frac{1 - \tau_\alpha}{C(1 - \tau_\beta) - (1 - \tau_\alpha)} \right]$$

where τ_α and τ_β are total atmospheric transmittances for channels α and β and $C = (T_s - \overline{T_\beta}) / (T_s - \overline{T_\alpha})$. Solving for $(T_\alpha - T_\beta)$:

$$(T_\alpha - T_\beta) = \frac{(T_s - T_\alpha)}{g(w)} \quad (2.9)$$

By using an approximation proposed by Prabhakara, et al.(1974):

$$(T_s - T_\alpha) \approx (T_s - \overline{T_\alpha}) K w \sec\theta \quad (2.10)$$

where θ is the scanning angle and K is an absorption coefficient. Column water vapor ($w = \int \rho_w dz$) ($g\ m^{-2}$) can be related to the brightness temperature difference:

$$(T_\alpha - T_\beta) \approx K \frac{(T_s - \overline{T_\alpha})}{g(w)} w \sec\theta \quad (2.11)$$

Although both $g(w)$ and $(T_s - \overline{T_\alpha})$ increase with increased water vapor, their ratio remains nearly constant (Dalu 1986). This leaves us with:

$$w = A(T_\alpha - T_\beta) \cos\theta \quad (2.12)$$

where $A = \text{const.} = (g(w))/(K(T_s - \overline{T_\alpha}))$.

To maximize the effectiveness of this scheme, T_α should be minimally influenced by water vapor in the atmosphere to allow the retrieval of water vapor temperatures near the surface. T_β , on the other hand, should be more sensitive to the atmospheric water vapor distribution. Under such conditions, $(T_\alpha - T_\beta)$ would indicate the influence of water vapor, which would be proportional to the amount (w).

Channel 4 ($\sim 11\mu\text{m}$) and channel 5 ($\sim 12\mu\text{m}$) windows of the AVHRR were designed for sensing of the sea surface temperature (SST) corrected for atmospheric absorption (Dalu 1986). Despite being optimized for SST retrieval, they describe a linear function from which the atmospheric water vapor correction can be derived (McMillin and Crosby 1984). Figure 5 shows

NOAA-7 AVHRR channels 4 and 5 response function curves superimposed on three model atmosphere τ of varying water vapor amounts. Notice that τ_4 is generally greater than τ_5 , leading to a positive T_4-T_5 , and that higher T_4-T_5 correlates directly with higher water vapor densities (Tropical > US Standard > Midlatitude Winter).

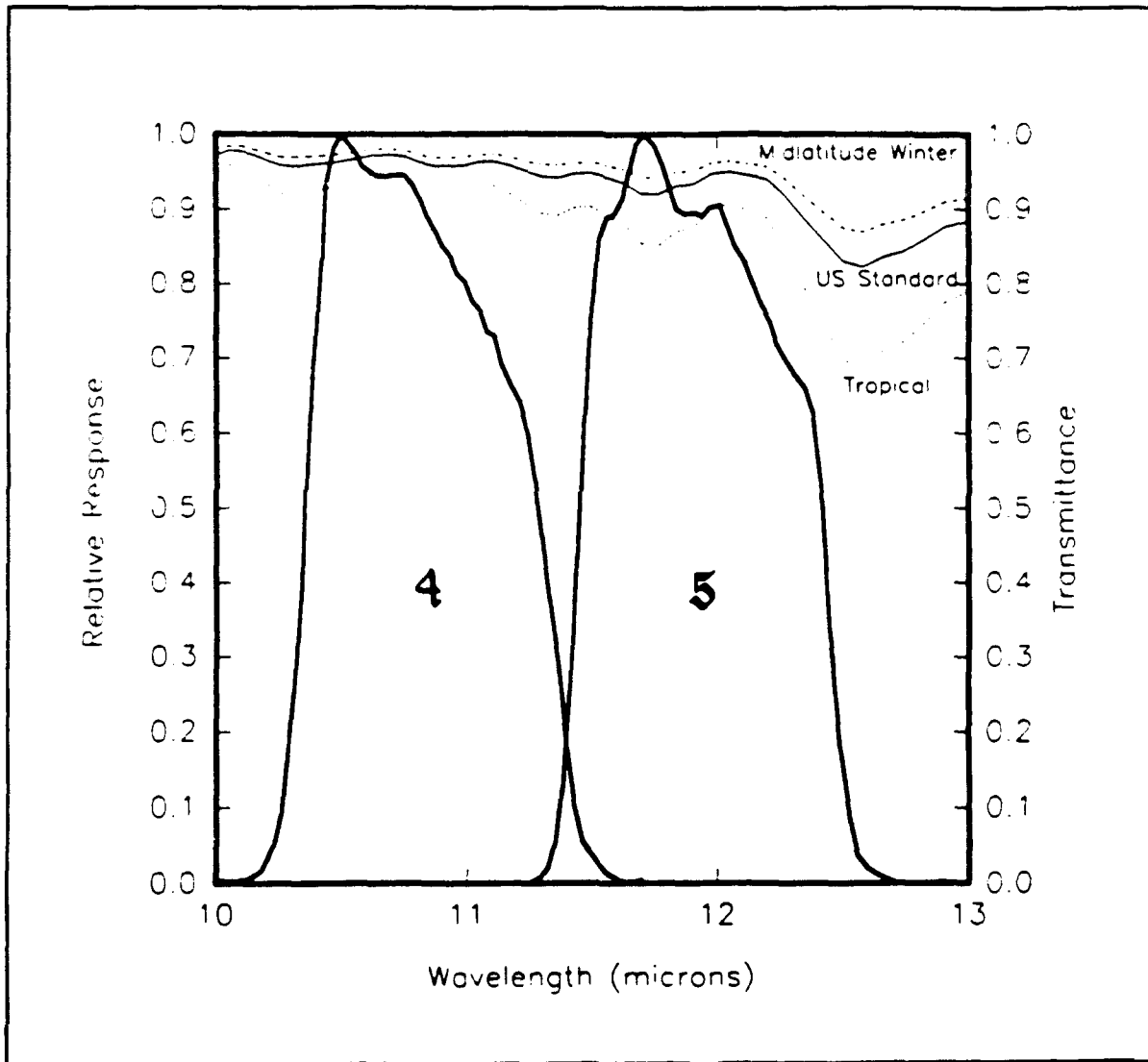


Fig. 5 NOAA-7 AVHRR channel 4 and 5 response functions and atmospheric transmittance due to water vapor.

Although not the ideal sensor windows for water vapor retrieval (the channels are too similar), the use of T₄-T₅ is justified to within the accuracy of the approximations made to achieve Eqn. 2.12. The most beneficial aspect of T₄-T₅ is the co-location and temporal linkage with channels 1 and 2, providing a water vapor snapshot simultaneously and using the same path as the aerosol optical depth (δ) measurements.

Therefore, an estimate of vertically integrated water vapor density (w) is provide by:

$$w = A^*(T_4 - T_5)\cos\theta \quad (2.13)$$

Using $A^* = 19600 \text{ g /}(\text{°K m}^2)$ and a scanning angle $\theta = 0$, Dalu (1986) applied this relationship to a radiative transfer model using a variety of temperature and humidity profiles. Figure 6 shows the correlation coefficient for the resulting line is $R = 0.99$ with the error given as $\pm 1.5 \text{ kg m}^{-2}$. Comparing results calculated using radiosonde data with shipboard measured water vapor amounts, Figure 7 shows the correlation coefficient dropped to $R = 0.78$ with an error of $\pm 4.0 \text{ kg m}^{-2}$. The decrease in accuracy most likely resulting from calibration errors as well as inexact temporal and spatial correlation of ship and satellite data.

At channel 4 and 5 wavelengths, scattering is a relatively insignificant influence determining brightness temperature (T). The dominant factor is water vapor absorption of surface temperatures.

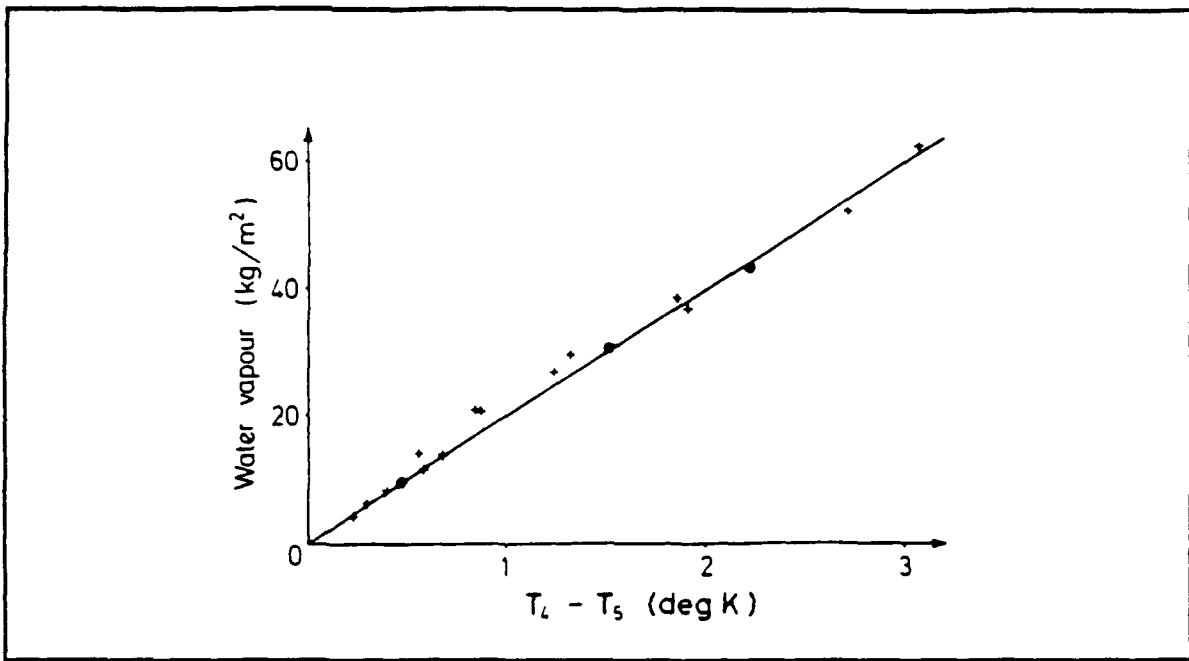


Fig. 6 Total water vapor content (kg/m²) as a function of brightness temperature difference from Dalu (1986).

Some of the long wave radiation emitted by the sea surface is absorbed by water vapor. The vapor then re-emits radiation based on temperature in accordance with the Planck function. If the atmosphere, and the water vapor included, were not generally cooler than the sea surface, the absorbed radiation would be re-emitted at the same rate, not having any effect on radiance or brightness temperature.

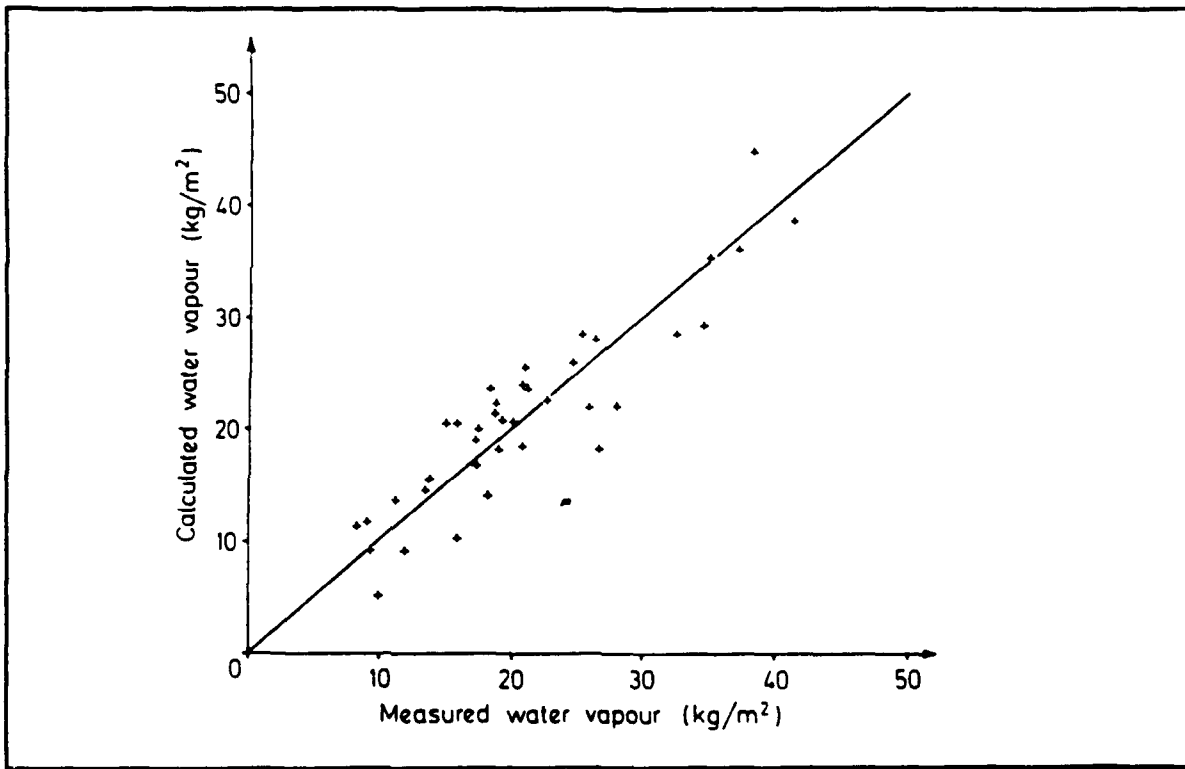


Fig. 7 Comparison of water vapor content from ships with radiative transfer model runs using ship radiosonde data. From Dalu (1986).

III. PROCEDURE

A. INTRODUCTION

This study uses the **LOWTRAN7** model to improve algorithms used in satellite retrieved optical depth measurements, specifically a correction due to varying amounts of water vapor present. The benefit in using a theoretical model is that the parameters involved can be specifically quantified and controlled. Therefore, a precise relationship between satellite measured radiances (L , w/cm^2 -steradian- cm^{-1}) and varied parameters such as optical depth (δ), atmospheric temperature (T , $^{\circ}K$), column water vapor (w , $gm\ m^{-2}$) can be determined. These relationships will be consistent with that of the real atmosphere to the degree that the model represents the real atmosphere.

B. OVERVIEW

Figure 8 is a flow chart of the procedure beginning with a user defined atmosphere of known quantities of aerosol optical depth (δ), water vapor densities (ρ_w), and surface temperatures (T_{surf}). Three programs are run for each data set. Both **LOWTRAN7** and its filter function program, **LOWFIL7**, make use of formatted files (**TAPEX.DAT**) for input, output, and to pass coded information between the programs. The program **RETRIEVE** was specifically designed for this study, to compile data in a condensed format.

LOWTRAN7 is supplied a modeled atmosphere, sun/satellite/earth geometry, as well as a desired wavenumber (κ) band. Wavenumber dependent

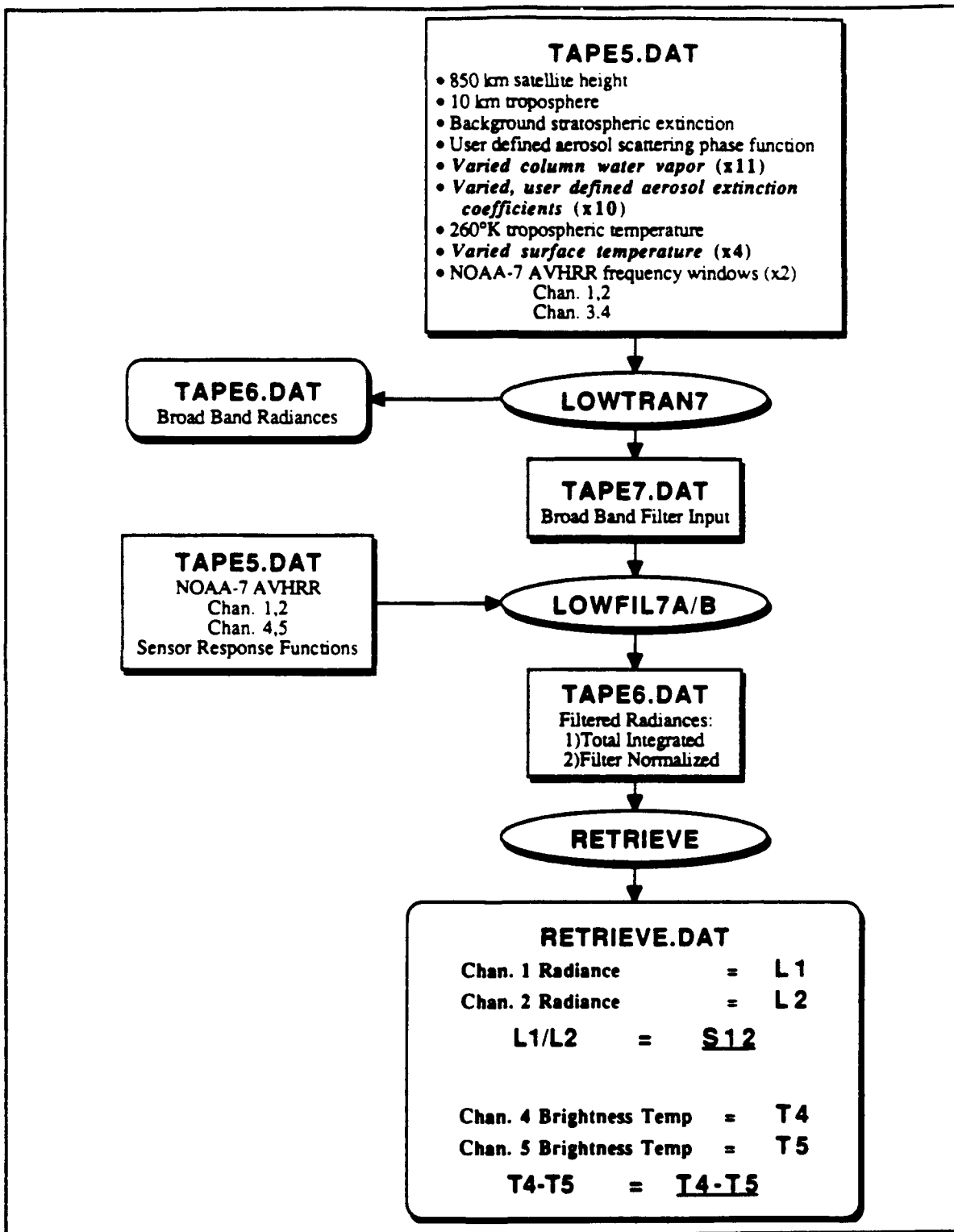


Fig. 8 Flow chart of model run.

radiances are calculated considering scattered, absorbed, and emitted radiation as it would be "seen" by a perfect sensor at the satellite location. Figure 9 shows the AVHRR sensor response function curves ($\Phi(\kappa)$) that LOWFIL7 combines with coded information derived from the previous LOWTRAN7 run to calculate the effective filtered radiances as a function of wavenumber or wavelength. The sensor weighted total integrated radiance is then determined.

$$L_{\text{tot}} = \int L(\kappa)\Phi(\kappa)d\kappa \quad (3.1)$$

LOWFIL7 was modified for use in this study to calculate the integral of the sensor's response function which is then used to calculate a normalized radiance (LOWFIL7A/B).²

$$L(\text{chan}) = \frac{\int L(\kappa)\Phi(\kappa)d\kappa}{\int \Phi(\kappa)d\kappa} \quad (3.2)$$

The program RETRIEVE reads the output files from LOWFIL7A/B and writes only the normalized radiances for channels 1, 2, 4, and 5 (L_1, L_2, L_4, L_5). The ratio of channel 1 to channel 2 radiances is calculated to determine the particle size index parameter (S_{12}) (Frost 1988).³

$$S_{12} = \frac{(L)_{\text{red}}}{(L)_{\text{nir}}} = \frac{L_1}{L_2} \quad (3.3)$$

²LOWFIL7 normalizes by , Φ_{max} instead of $\int \Phi(\kappa)d\kappa$.

³Unlike Frost, this study does not first remove L_r .

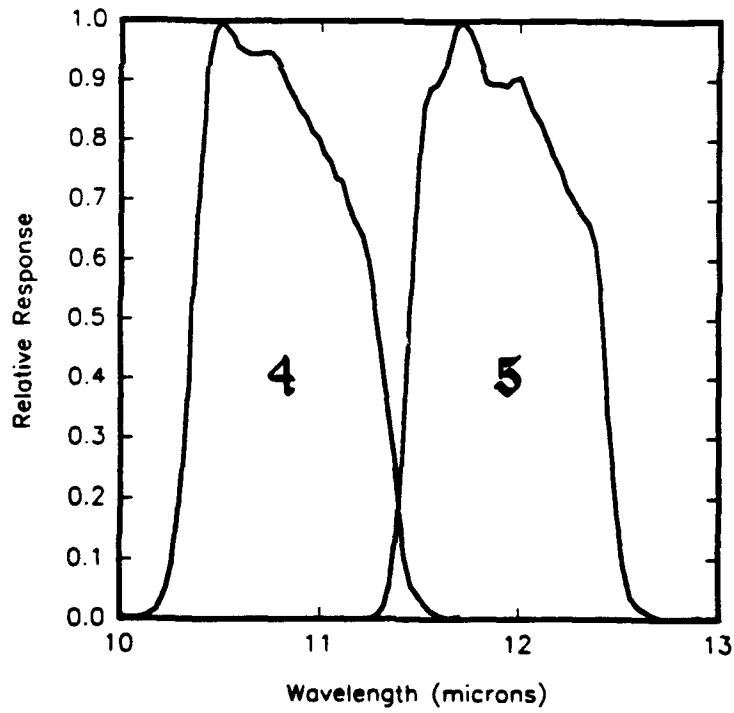
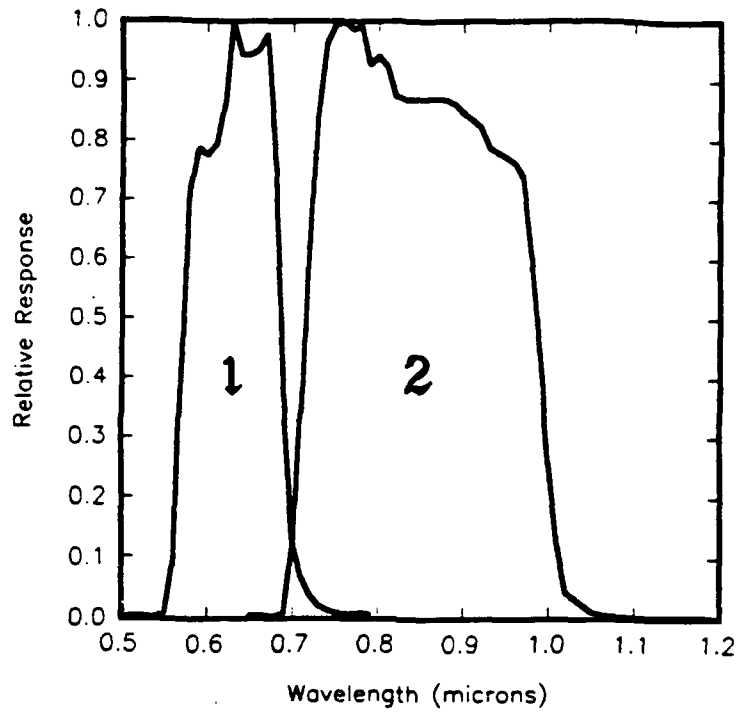


Fig. 9 NOAA-7 AVHRR filter function response curves.

Channel 4 and channel 5 radiances are converted to brightness temperatures (T_b).

$$T_{b(4,5)} = \frac{C_2 \kappa}{\ln \left(1 + \frac{C_1 \kappa^3}{L(\text{chan } 4,5)} \right)} \quad (3.4)$$

Where $T_{b(4,5)}$ is the brightness Temperature (K) for the radiance $L(4,5)$ (w/cm^2 -steradian- cm^{-1}), κ is the central wavenumber of the channel filter ($\kappa_{\text{chan4}} = 927.22 \text{ cm}^{-1}$ and $\kappa_{\text{chan5}} = 840.872 \text{ cm}^{-1}$), and C_1 and C_2 are constants ($C_1 = 1.1910659 \times 10^{-12} \text{ w/cm}^2$ -steradian- cm^{-4} and $C_2 = 1.438833 \text{ cm}^{-1} \text{ K}$) (NOAA Polar Orbiter Data 1986). Finally, the brightness temperature difference between T_{b4} and T_{b5} is calculated ($T_4 - T_5$).

C. INPUT CHARACTERISTICS

The modeled atmospheres were restricted to cloud-free marine environments where backscattered radiance is dominated by aerosol particles (Durkee 1984). Since the satellite senses the effect of vertically integrated parameters, the models used were homogeneous from the surface to the tropopause. For ease of integration, the model tropopause was set to 10 kilometers (the average height of the mid-latitude tropopause is about 11 kilometers (Stull 1988)). From the tropopause to the satellite height, only background extinction due to meteoric dust is represented from 30 to 100 kilometers. The following are the important user-defined parameters:

aerosol optical depth ($\delta_a(\lambda)$)	varied
column water vapor (w)	varied
tropospheric air temperature (T_{air})	260 K
surface temperature (T_{surf})	varied

surface albedo (**Salb**)0.0 (blackbody)
 satellite height (**H**)850 km
 season spring-summer
 marine phase function (**P(Θ)**)..... from Shettle and Fenn (1979)
 wavenumber windows, resolution
 chan 1,28400--20050 cm⁻¹, 50 cm⁻¹
 chan 4,5770--1005 cm⁻¹, 5 cm⁻¹

Molecular constituents such as O₃, CH₄, N₂O, CO, CO₂, O₂, NO, SO₂, NO₂, NH₃, and HNO₃, used **LOWTRAN7** model default profiles for midlatitude summer and were kept constant for all model runs. The sun/satellite geometry remained the same throughout all the model runs with the satellite and sun in a straight line perpendicular to the earth's surface.

1. Optical Depth Profiles

Satellite windows in the red-visible and near-infrared sense the result of vertically integrated parameters. The most significant influence on retrieved radiances is the vertical integral of σ_{ext} or δ . To study this effect, ten profiles of δ with constant σ_{ext} to 10 km were designed.

Using the relationship

$$\sigma_{\text{scat}} \propto \lambda^{-1.5} \tag{3.5}$$

and an σ_{scat} of .05 km⁻¹ at $\lambda = .55 \mu\text{m}$, a profile of σ_{scat} as a function of λ was derived ($\sigma_{\text{scat}}(\lambda)$). After integrating over the 10 km height to determine δ , Figure 10 shows this curve (M2) and four multiples of this profile that complete the first set of optical depth profiles.

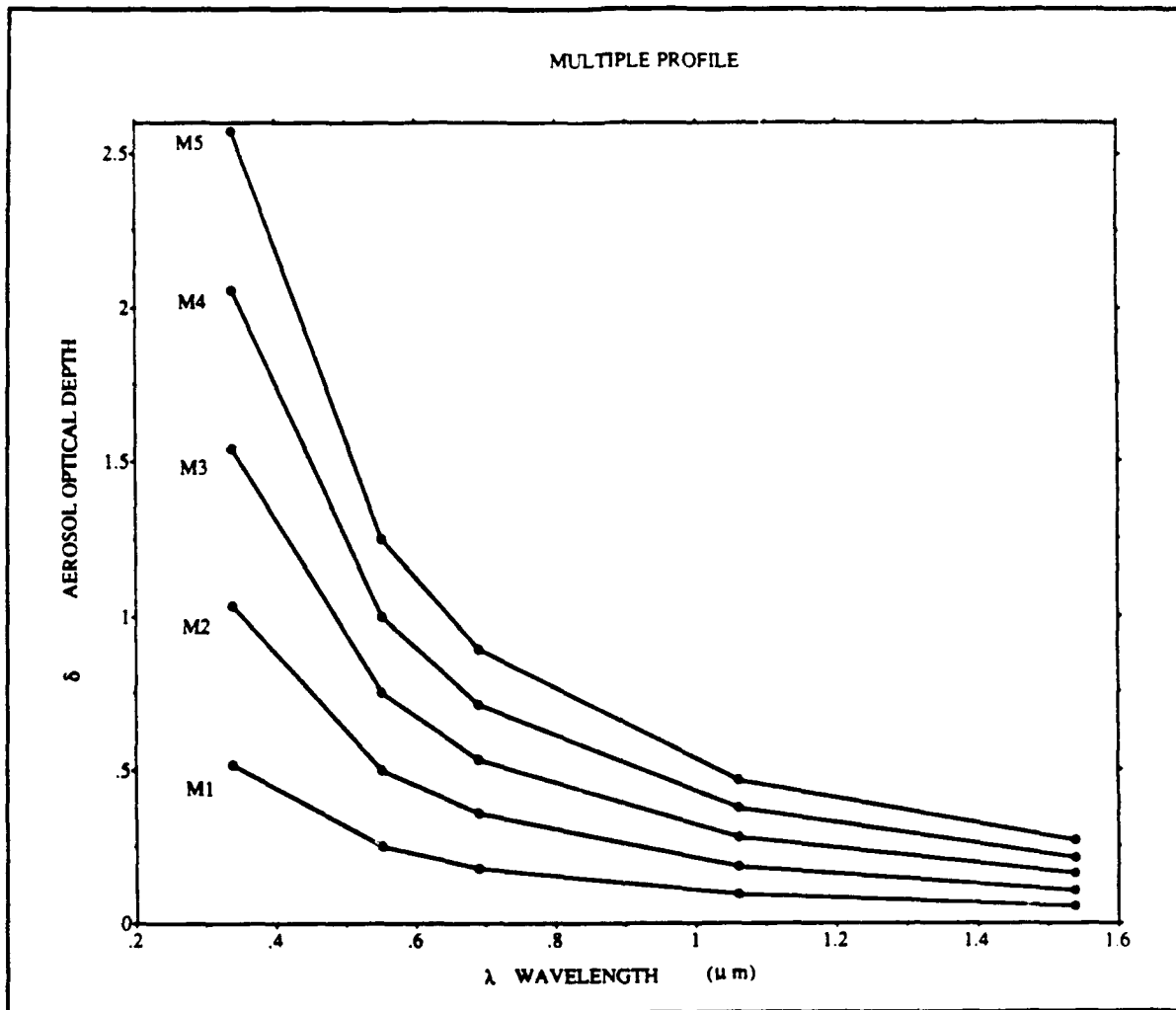


Fig. 10 Multiple optical depth profiles (M).

Figure 11 shows a second set of profiles created using the same relationship and adding equal quantities to create parallel profiles.

2. Water Vapor

All the water vapor was contained in the homogeneous troposphere (0 to 10 km). The maximum value was selected from the tropical atmosphere model included in **LOWTRAN7** (3.322 gm cm^{-2}). User-defined profiles are input as water vapor mass density (ρ_w) (gm m^{-3}), which after integrating in the

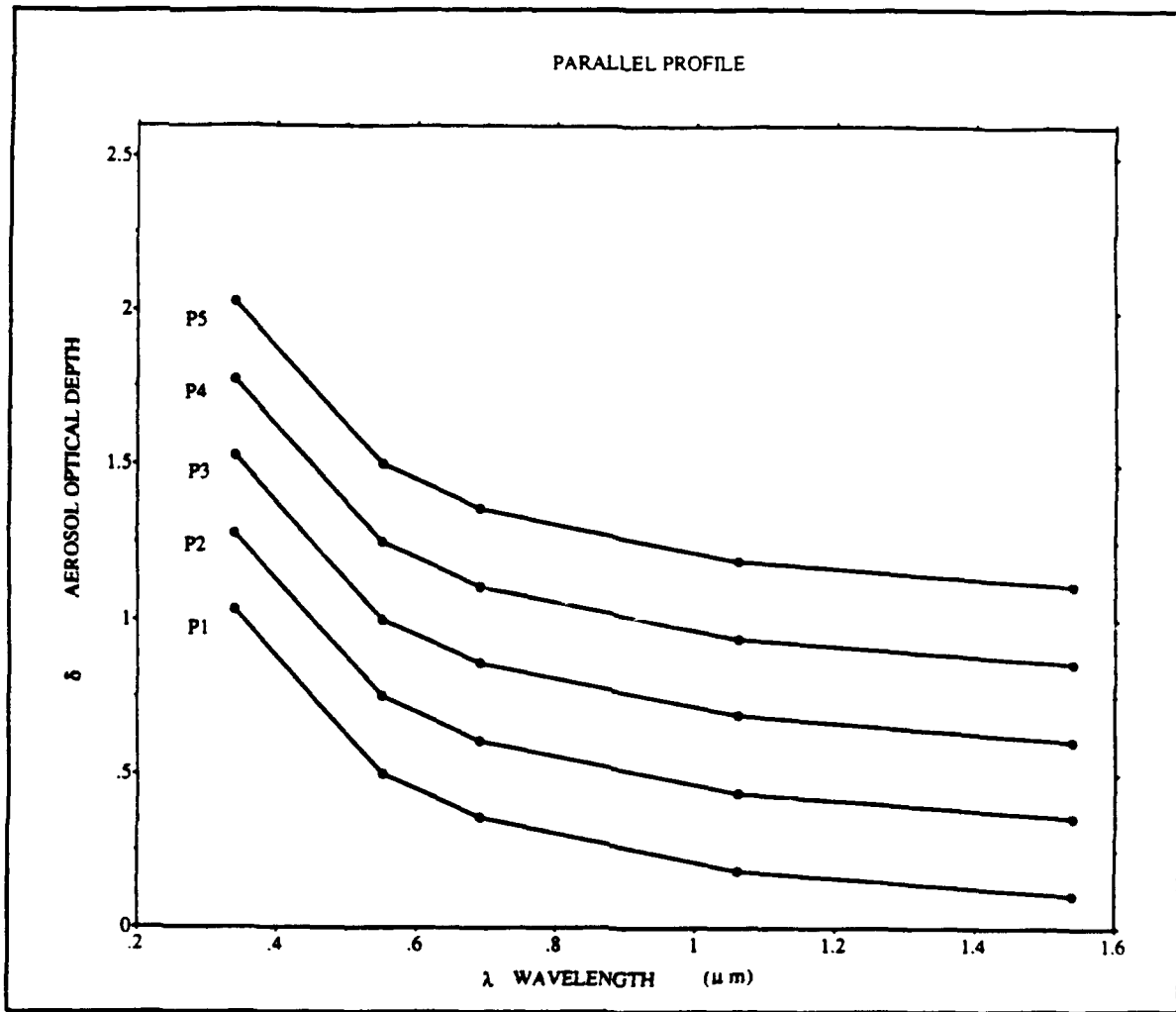


Fig. 11 Parallel optical depth profiles (P).

vertical gives column water vapor (w) of equivalent magnitudes in units of gm cm^{-2} .

$$w = \int_0^H \rho_w dz \quad (3.6)$$

Ten intermediate quantities between 0 and 3.322 gm cm^{-2} were selected with 0 included as the eleventh.

3. Surface Temperature

T_4 - T_5 is a measure of water vapor (Jacobowitz and Gruber 1990) and will be compared with the user input water vapor concentrations, as an empirical method of estimating w . T_5 is more sensitive to water vapor effects on atmospheric transmittance while T_4 senses more of the near-blackbody, long-wave radiation from the surface. In order to demonstrate relationships, the model required a warmer surface temperature than the atmosphere when the troposphere is isothermal. With equal atmospheric temperature (T_{atm}) and surface temperature (T_{surf}), the measured brightness temperatures would be identical. Also, surface temperatures colder than the temperature at 10 km are unrealistic. Therefore, while the tropospheric temperature was held constant, the surface temperature was varied to achieve four representative modeled T_{atm}/T_{surf} relationships:

T_{atm}	260°K
$T_{surf}(w)$	270°K
$T_{surf}(x)$	280°K
$T_{surf}(y)$	290°K
$T_{surf}(z)$	300°K

D. PROCEDURAL SUMMARY

The model was run at the Naval Postgraduate School's (NPS) Interactive Environmental Digital Analysis Laboratory (IDEA LAB). A complete set of input files consisted of two sets of five δ profiles, with eleven w variations, four surface temperature conditions, and two wavenumber windows. These 880 files (2 X 5 X 11 X 4 X 2) generated 1760 intermediate and final output files, with the significant data 'retrieved' and collated in one resultant array. All the

calculations were done as a large batch job requiring about 4.5 hours to run. The job was completed in both the single and multiple aerosol scattering modes of **LOWTRAN7**.

IV. RESULTS

A. THE EFFECT OF AEROSOL OPTICAL DEPTH VARIATIONS ON S_{12}

In general, an increase in wavelength dependant aerosol optical depth ($\delta_a(\lambda)$) resulted in an increase in L_1 and L_2 while S_{12} values decreased. Since S_{12} is generally greater than one ($L_1 > L_2$). Increasing the radiance in both sensor windows by similar magnitudes has a greater influence on the smaller L , driving S_{12} toward one. This relationship will remain true because of the Rayleigh contribution, which is greater for L_1 .

1. Multiple $\delta_a(\lambda)$ Scheme

Increasing δ_a profiles result in decreasing S_{12} ratios, with the rate of decrease diminishing due to the effect of increasing $\delta_a(\lambda)$ slopes. Figure 12 shows the S_{12} variations resulting from the multiple δ_a profiles of Fig. 10.

2. Parallel $\delta_a(\lambda)$ Scheme

By constraining the curves to be parallel, an increase in δ_a is an equal increase at all wavelengths. The S_{12} ratios decrease at a more rapid rate than in the previous scheme since a change in slope is no longer limiting the decrease in S_{12} . Figure 13 shows the S_{12} variations resulting from the parallel δ_a profiles of Fig. 11.

B. THE EFFECT OF SURFACE TEMPERATURE VARIATIONS ON THE T_4 - T_5 REPRESENTATION OF w

Although the modeling accomplished in this study was not designed to prove Dalu's technique for determining vertically integrated water vapor density (w) from T_4 - T_5 , some significant aspects of his theory are supported by the results.

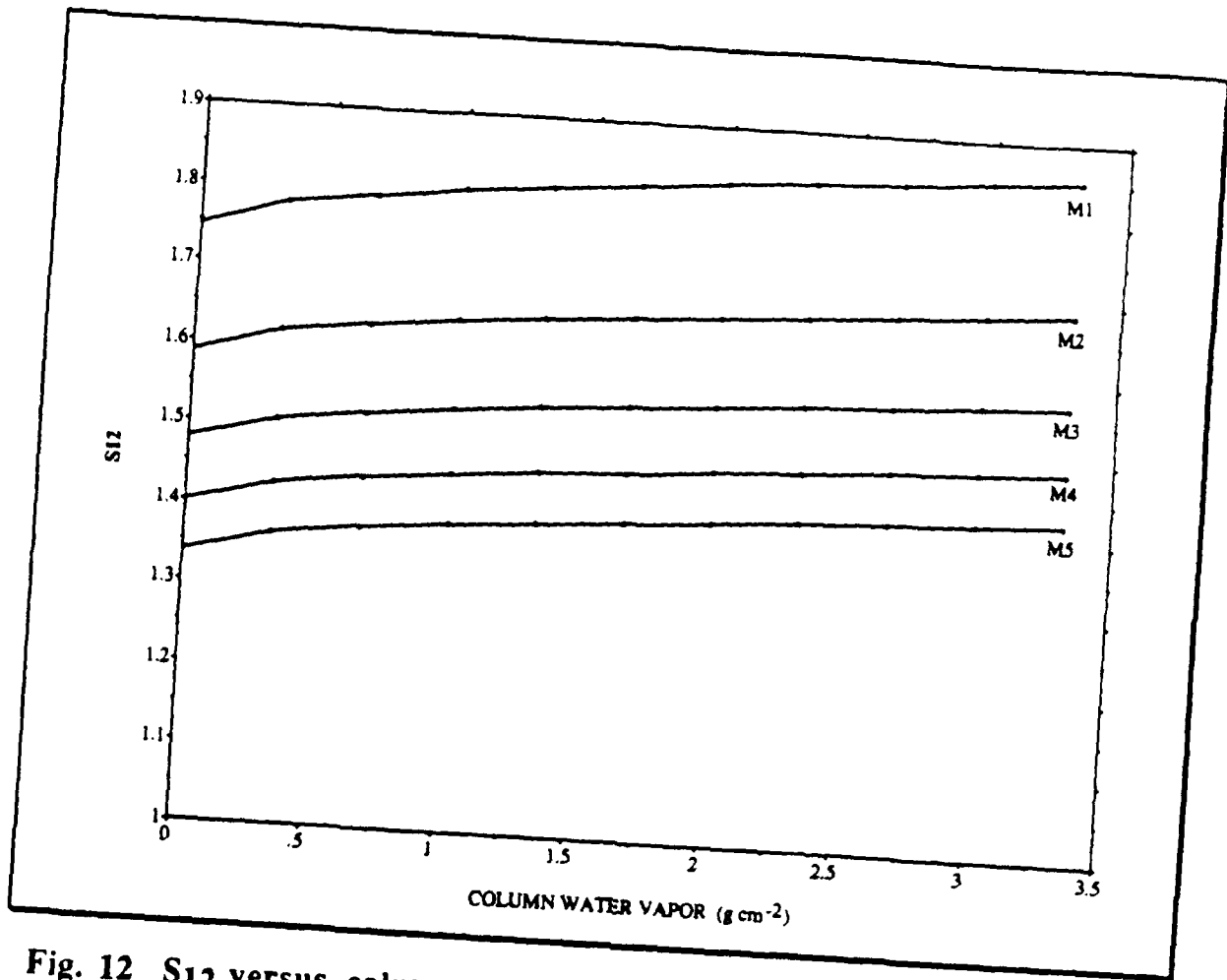


Fig. 12 S_{12} versus column water vapor (w) for the multiple optical depth scheme (M).

Figure 14 shows the T_4-T_5 values derived from modeled atmospheres of known w given a 260K isothermal air temperature (T_{air}) and various T_{surf} conditions. The slopes of the T_4-T_5 varied from Dalu's estimate, yet the linear relationship of Eqn. 2.13 seemed evident.

The variation in the slopes is a result of the assumptions made in the model atmospheres. The use of an isothermal 10 km atmosphere is reasonable for NOAA-7 AVHRR channel 1 and 2 retrievals since these wavelengths

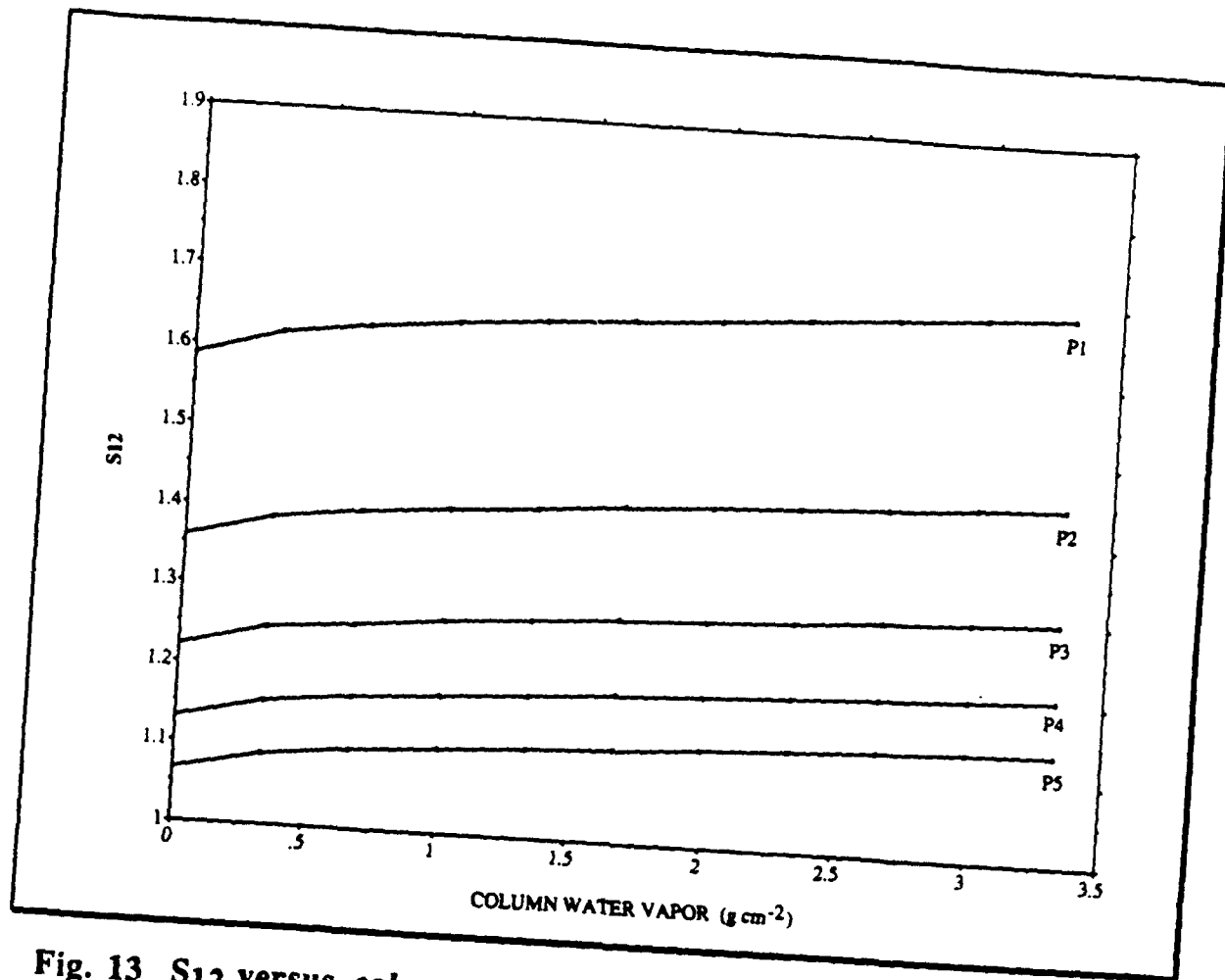


Fig. 13 S_{12} versus column water vapor (w) for the parallel optical depth scheme (P). (red-vis, nir) sense the vertically integrated aerosol backscattering with little height dependence. Since absorption plays a big role in channel 4 and 5 brightness temperature retrievals in the actual atmosphere, T_{b4} and T_{b5} results are significantly influenced by vertical temperature variations. The isothermal assumption used in this model study, therefore, causes quantitative T_4 - T_5 results to be unrepresentative of the real atmosphere. However, qualitative results such as the linear relationship are retained. Table 2 compares the slopes derived from applying Dalu's theory to each T_{air}/T_{surf} variation.

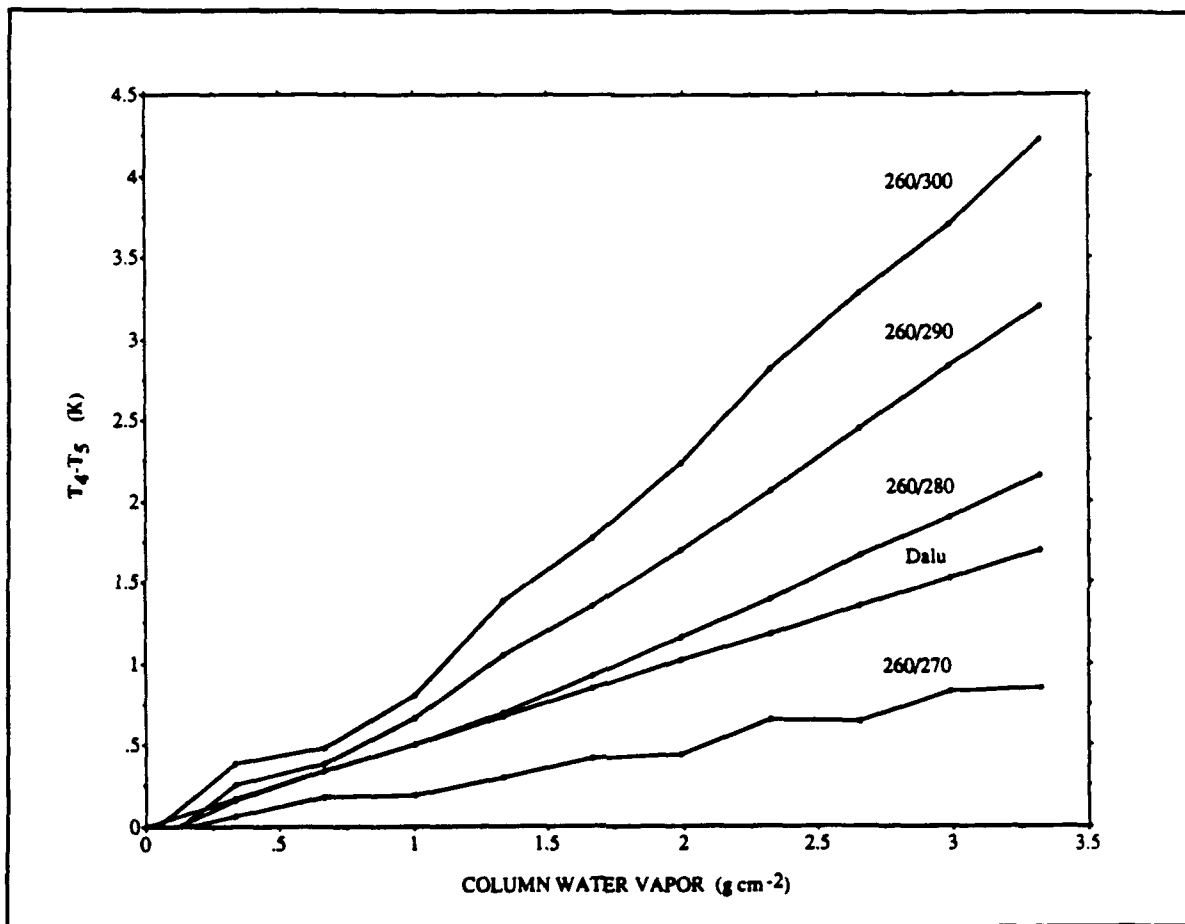


Fig. 14 $T_4 - T_5$ versus column water vapor (w) for a variety of surface temperatures.

TABLE 2
MODEL OUTPUT COEFFICIENTS APPLIED TO DALU'S
THEORY ($w = A(T_4 - T_5)$)

T_{air}/T_{surf} (K/K)	A (g K ⁻¹ m ⁻¹)
260/300	.7615
260/290	.9944
260/280	1.4995
260/270	3.6653
Dalu	1.9600

C. THE W CORRECTION TO S₁₂

In order to present the correction to satellite retrieved S₁₂ values required due to the presence of water vapor, the results will be displayed first graphically, then in a new parameterization that can be applied to the aerosol scattering phase functions used in retrieval of aerosol characteristics from satellites.

1. Graphical Application

RETRIEVE lists the following results for each modeled atmosphere:

Input Parameters:

$\delta_a(\lambda)$
 T_{surf}
 w

Output Variables:

$L_1\}$
 $L_2\} \Rightarrow S_{12}$

$T_{b4}\}$
 $T_{b5}\} \Rightarrow T_4 - T_5$

A set of output variables was calculated for each variation of input parameters. The combined results are displayed in Fig. 15.

To use this figure to determine S_{12} corrected for w : Begin with NOAA-7 AVHRR retrieved data (S_{12} , T_4-T_5). Read T_4-T_5 value on lower half of plot and look for the intersection with Dalu curve. This will determine column water vapor. Move up (parallel to the grid lines), to the satellite measured S_{12} value. Follow the contours of the nearest curve to the S_{12} axis and read $S_{12}(\text{dry})$. This will be the S_{12} with the effects of water vapor in the column removed.

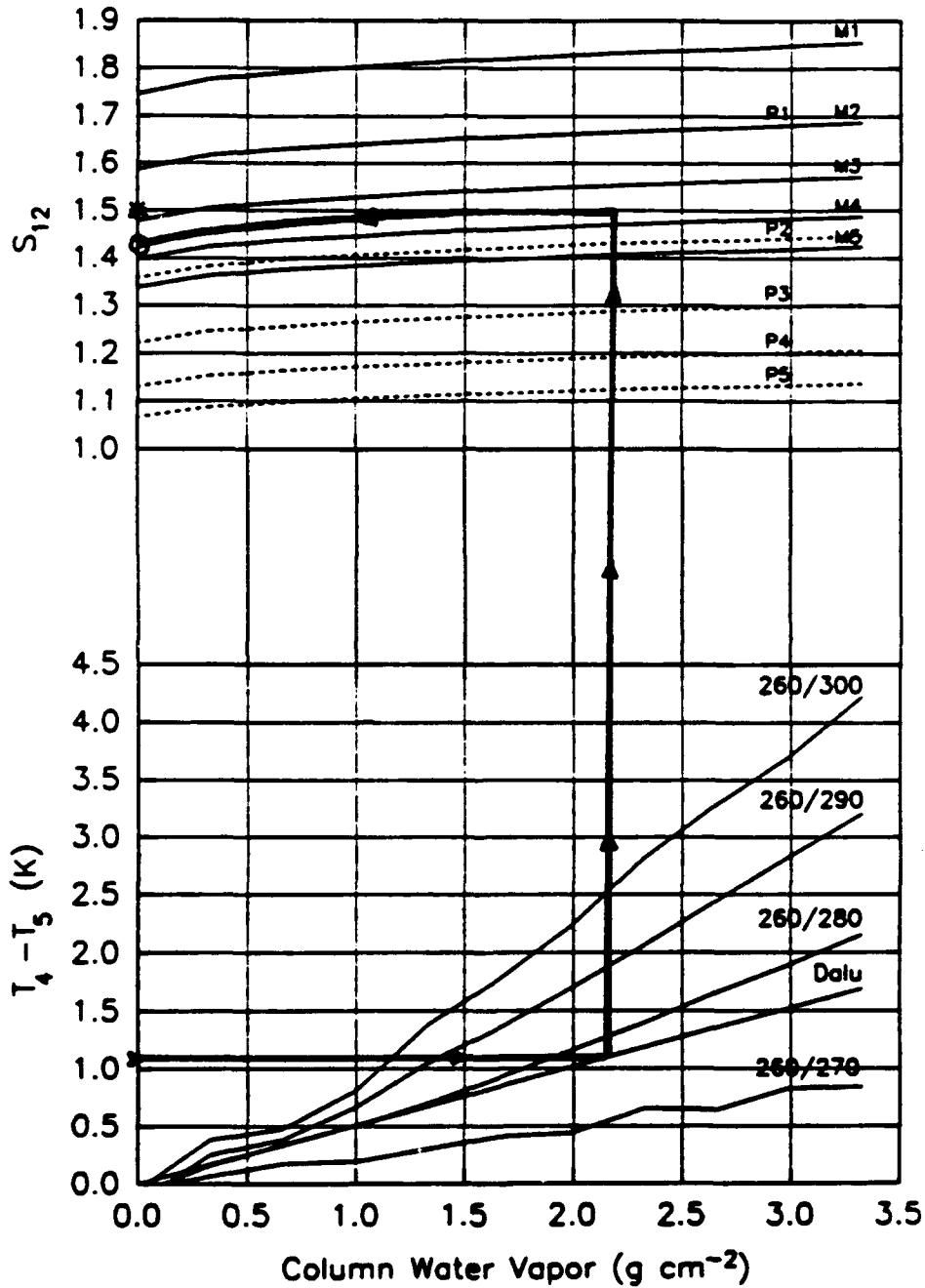


Fig. 15 S_{12} correction for column water vapor.

Both the multiple and parallel S_{12} results are displayed and seem to follow a similar relationship to w . Note that M2 and P1 curves are coincident. They use the same input $\delta_a(\lambda)$ values that formed the basis for each set of curves.

2. The Reformulated Parameterization

Looking at the S_{12} values plotted for varying w and $\delta_a(\lambda)$ curves, there appears to be a functional relationship. It is apparent that the water vapor influence of S_{12} is not dependent on the shape of the optical depth profile, but was a function of w and the magnitude of S_{12} when $w = 0$ ($S_{12}(\text{dry})$). Figure 16 shows that when the ratio of $S_{12}:S_{12}(\text{dry})$ was plotted as a function of w , the shape of the curve was conserved for all model outputs (multiple and parallel). The slight variation at higher w is partly due to computational round off errors. The curve that best fits the data is:

$$S_{12}(\text{dry}) = (1 + .0332 \sqrt{w}) S_{12} \quad (4.1)$$

with $r^2 = 0.995$.

From Eqn. 4.1, measured S_{12} and estimated w from T_4 - T_5 determines $S_{12}(\text{dry})$.

D. SINGLE VERSUS MULTIPLE SCATTERING

All data sets were run with both single scatter and multiple scatter approximations. The results were calculated to the seventh decimal place and were precisely the same for either case. The model, therefore, supports Frost's use of a simplified form of the Radiative Transfer Equation (RTE) that assumes single scatter (Eqn. 2.1).

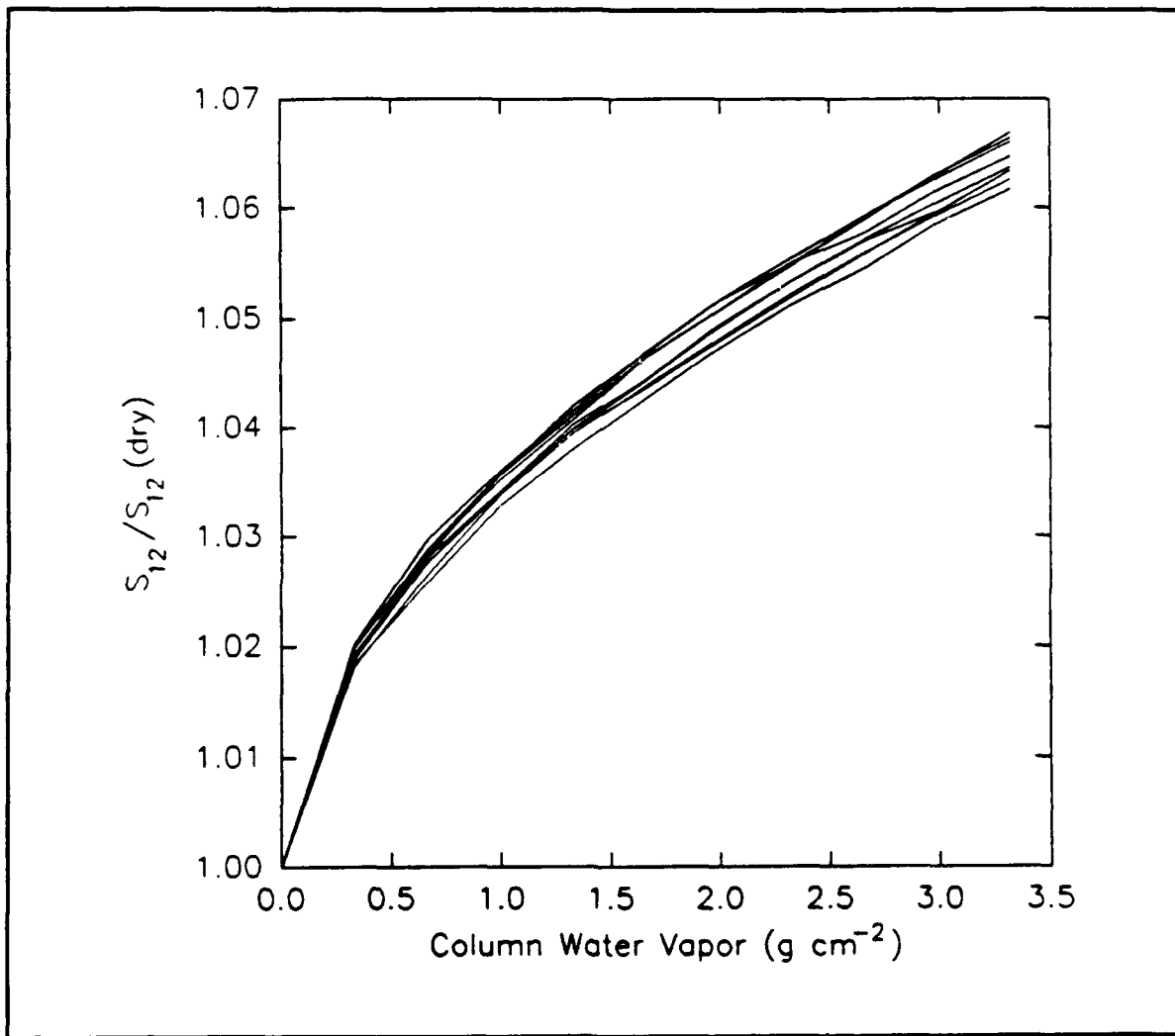


Fig. 16 S_{12} normalized by $S_{12}(\text{dry})$.

V. CONCLUSIONS

Present techniques for satellite retrieval of aerosol characteristics using the AVHRR carried on the NOAA series platforms require that analyzed pixels be free of clouds. This is reasonable since liquid water effects on radiative processes are quite variable and difficult to measure. Clouds at any level in a satellite scene can obscure the sources it was designed to sense, or saturate the sensor with reflected radiance. It is understood that water in a gaseous form would still be present, but its influence on L in the wavebands most effectively used to estimate aerosol parameters (Chan. 1 and Chan. 2) has been assumed to be insignificant in previous studies.

Although aerosol scattering is still the dominant influence on L in these wavebands, this study has shown that water vapor does introduce an error, and that the error can be removed. This does not invalidate the present techniques, but provides a significant improvement that can be applied through the use of the variable scattering phase function introduced by Frost (1988). Since aerosol variations can be of global scale, even very small changes may have global ramifications.

Through the use of the LOWTRAN7 atmospheric propagation model, this study has shown support of the following techniques and theories presently accepted:

- The concepts of Frost's particle size index parameter (S_{12}) using AVHRR channels 1 and 2.
- Frost's use of a simplified radiative transfer equation based upon an assumption of single scatter.
- Dalu's water vapor retrieval technique using AVHRR channels 4 and 5

By introducing varying quantities of water vapor to the modeled atmospheres of differing optical depth (δ) and $T_{\text{surf}}/T_{\text{air}}$ profiles, additional information has been generated:

- The error introduced to S_{12} due to water vapor is demonstrated and quantified.
- The error has been shown to be a function of $S_{12}(\text{dry})$ and column water vapor (w).

The influence of optical depth variations can be isolated from the variation due to w through the use of the variable scattering phase function ($P(\Theta)$) proposed by Frost, (1988). Using Eqn. 2.1, S_{12} with 2.0gm cm^{-2} of water vapor produces a 15% error in $P(\Theta)$ and therefore retrieved aerosol optical depth (δ_a).

By using a model to determine water vapor's influence on satellite-measured aerosol characteristics, the parameters normally estimated can be strictly controlled. As known quantities, their theoretical relationships to satellite-measured quantities can be observed. The next step is to apply the correction discovered here to empirical satellite data with verifying in situ data sources such as aircraft or ships.

LIST OF REFERENCES

- Bloembergen, N., Patel, C. K., and G. Pake (Chairpersons), 1987: Science and Technology of Directed Energy Weapons. Report of the American Physical Society Study Group, *Reviews of Modern Physics*, **59**, S1-S202.
- Charlson, R.J., Lovelock, J.E., Andrea, M.O., and S.G. Warren, 1987: Oceanic Phytoplankton, atmospheric sulfur, cloud albedo and climate. *Nature*, **325**, 655-661.
- Dalu, G., 1986: Satellite Remote Sensing of Atmospheric Water Vapor. *International Journal of Remote Sensing*, **7**, 1089-1097.
- Dalu, G., Prabhakara, C., and Lo, R. C., 1981: Improved accuracy of the remote sensing of sea surface temperature. *Oceanography from Space*, J. F. R. Gower, ed., New York:Plenum, 109.
- Durkee, P.A., 1984: *The relationship between marine aerosol particles and satellite-detected radiance*. Ph.D. dissertation, Colorado State University, Fort Collins, CO, US ISSN 0067-0340, 124pp.
- Frost, E.M., 1988: *Global scale estimates of aerosol particle characteristics*. M.S. Thesis, Naval Postgraduate School, Monterey, CA., 54pp.
- Griggs, M., 1979: Satellite Observations of Atmospheric Aerosols During the EOMET Cruise. *Journal of Atmospheric Science*, **36**, 695-698.
- Jacobowitz, H., and A. Gruber, 1990: *Estimation of the Outgoing Longwave Flux from NOAA AVHRR Satellite Observations*. Seventh Conference on Atmospheric Radiation. American Meteorological Society, 4pp.
- McMillin, L. M., and D. S. Crosby, 1984: Theory and Validation of the Multiple Window Sea Surface Temperature Technique. *Journal of Geophysical Research*, **89**, 3655-3661.
- NOAA POLAR ORBITER DATA (TIROS-N, NOAA-7, NOAA-8, NOAA-9 AND NOAA-10) Users Guide**. U. S. Department of Commerce, National Oceanic and Atmospheric Administration, December 1986.

- Pfeil, F. R., 1986: *Developing a physical basis for an aerosol climatology of the Pacific Ocean*. M.S. Thesis, Naval Postgraduate School, Monterey, CA, 76pp.
- Prabhakara, C., Dalu, G., and Kunde, V. G., 1974: Estimation of sea surface temperature from remote sensing in the 11 to 13 μm window region. *Journal of Geophysical Research*, 79,5039.
- Ramsey, R. C., 1968: Study of the Remote Measurement of Ocean Color. Final Report, TRW, NASW-1658.
- Shettle, E. P., and R. W. Fenn, 1979: *Models for the Aerosols of the lower Atmosphere and the Effects of Humidity Variations on Their Optical Properties*. AFG-TR-79-0214 Air Force Geophysics Laboratories, Hanscom AFB, MA., 94pp.
- Stull, R. B., 1988: *An Introduction to Boundary Layer Meteorology*. Kluwer Academic Publishers, Dordrecht, The Netherlands, 666 pp.

INITIAL DISTRIBUTION LIST

	No. Copies
1. Defense Technical Information Center Cameron Station Alexandria, VA 22314	2
2. Library, Code 52 Naval Postgraduate School Monterey, CA 93943-5000	2
3. Chairman (Code OC/Co) Department of Oceanography Naval Postgraduate School Monterey, CA 93943-5000	1
4. Chairman (Code MR/Hy) Department of Meteorology Naval Postgraduate School Monterey, CA 93943-5000	1
5. Professor P. A. Durkee (Code MR/De) Department of Meteorology Naval Postgraduate School Monterey, CA 93943-5000	1
6. Professor K. L. Davidson (Code MR/DS) Department of Meteorology Naval Postgraduate School Monterey, CA 93943-5000	1
7. LT Timothy P. Mahony, USN NAVOCEANCOMCEN Box 31 FPO New York, NY 09549-3200	1

8. **Commanding Officer** 1
Naval Oceanographic and Atmospheric
Research Laboratory
Stennis Space Center
MS 39529-5004

9. **Director** 1
Naval Oceanographic and Atmospheric
Research Laboratory
Monterey, CA 93943-5006

10. **Chairman** 1
Oceanography Department
U. S. Naval Academy
Annapolis, MD 21402

11. **Office of Naval Research (Code 420)** 1
Naval Ocean Research and Development
Activity
800 N. Quincy Street
Arlington, VA 22217

12. **Scientific Liaison Office** 1
Office of Naval Research
Scripps Institution of Oceanography
La Jolla, CA 92037

13. **NOAA Library** 1
7600 Sand Point Way NE
Building 3
Seattle, WA 98115